ChemElectroChem

Research Article
doi.org/10.1002/celc.202400550

Chemistry Europe
European Chemical Societies Publishing

www.chemelectrochem.org

Exploration of the High-Capacity Tetrahydroxybenzene Materials for Organic Batteries

Klemen Pirnat,*[a, b] Uroš Javornik,[a] Nerea Casado,[b] Nicholas Ballard,[b] Jose Ignacio Santos,[c] David Mecerreyes,[b, d] and Robert Dominko[a, e, f]

Polyphenol or multihydroxybenzene compounds show great potential as electrode material for organic batteries. Among them, 1,2,3,4-tetrahydroxybenezene is the best candidate as a high-specific capacity material due to its potential to exchange up to four electrons. To further corroborate this, we synthesized a model compound and carry out electrochemical characterization. Quasi-reversible redox behavior, similar to other hydroxybenzene materials, was obtained in an acidic aqueous electrolyte. The four electron exchange was further confirmed by using reduced and oxidized model compounds, which showed comparable electrochemical behavior. Additionally, we prepared insoluble nano sized polymer based on poly(2,3,4,5-tetrahydroxystyrene) which was used as a cathode material in an organic battery. Initial results suggested that these tetrahyroxybenzene polymers are very promising for proton batteries in acidic aqueous electrolytes, whereas their performance in lithium batteries is limited.

1. Introduction

Climate change and decreasing reserves of readily available and low-cost fossil fuels are prompting our society to shift toward renewable energy resources. With some investment, the production of renewable energy can meet our needs, but this production is time and location-dependent. This raises concerns about the stability of the energy supply and consequently the stability of the grid. The discrepancies between energy production and demand on a daily to weekly basis can be regulated with the help of intermediate storage. Currently, the main energy storage solutions rely primarily on pumped storage power plants, but this type of energy storage has a relatively low energy density and requires a suitable geographical configuration. Batteries offer an alternative with significantly higher energy density and are expected to play an increasingly important role in the future storage of electrical energy.

The most important factors for the acceptance of batteries for grid storage are price, sustainability, and durability. Li-ion battery technology is becoming increasingly important in this area, but its sustainability and scalability are questionable due to the use of rare elements (Co, Ni, Li) with strong price fluctuations. Alternatives to the current Li-ion battery technology are under development, such as Li–S, Li–O2, beyond-Li technologies (like Na-ion, Mg and Al batteries) and various metal – organic batteries. The metal-organic batteries are particularly interesting because organic positive electrodes have demonstrated reversible electrochemical performance with lithium and other monovalent cations (Na,[1] K[2]) and multivalent cations:[3,4] Mg,[5–14] Ca,[15–17] Zn[18,19,28,20–27] and Al.[29–33] This could play a crucial role in the future if we want to develop more sustainable batteries that are not dependent on critical raw materials. Organic positive electrodes are attractive since they can be produced from bio derived feedstock and organic waste at low temperatures. This can have a major impact on the reduced carbon footprint per kWh stored and improve their sustainability

Currently, organic batteries compete with Li-ion technology in terms of the gravimetric energy density (Wh/kg).[34–41] As their research is still in its infancy, we can expect further improvements. To increase the energy density of organic positive materials, we have a limitation with the upper voltage which is lower than 3.0 V vs. Li/Li^+ for n-type materials and 4.0 V vs. Li/Li^+ for p-type materials. The n-type materials are neutral in the oxidized state. After reduction, they become negatively charged and bind positive Li^+ cations. As the Li^+ cations come from the negative electrode, their concentration in the electrolyte remains stable. On the other hand, p-type materials are neutral in the reduced state and become positively charged after

[a] K. Pirnat, U. Javornik, R. Dominko
National Institute of Chemistry, Hajdrihova 19, 1000 Ljubljana, Slovenia
E-mail: klemen.pirnat@ki.si

[b] K. Pirnat, N. Casado, N. Ballard, D. Mecerreyes
POLYMAT University of the Basque Country UPV/EHU, Joxe Mari Korta Center, 20018 Donostia-San Sebastian, Spain

[c] J. I. Santos
NMR of Facility of Research (SGIker), University of the Basque Country (UPV/EHU), Avenida Tolosa 72, 20018 Donostia-San Sebastián, Spain

[d] D. Mecerreyes
Ikerbasque, Basque Foundation for Science, Maria Diaz de Haro 3, E-48011 Bilbao, Spain

[e] R. Dominko
Faculty of Chemistry and Chemical Technology University of Ljubljana Večna pot 113, 1000 Ljubljana, Slovenia

[f] R. Dominko
Alistore-European Research Institute CNRS FR 3104, Hub de l'Energie Rue Baudelocque 80039 Amiens, France

Supporting information for this article is available on the WWW under https://doi.org/10.1002/celc.202400550

oxidation and bind anions from the electrolyte, causing their concentration to fall during the charging process.[42,43] On the other hand, there is still room for improvement in the specific capacity. Carbonyl compounds are currently the best candidates and can theoretically achieve a specific capacity of up to 957 mAh/g for hexaketocyclohexane with six carbonyl groups. Theoretically, six electrons can be reversibly involved in the electrochemical reaction and form an aromatic benzene ring. In the presence of protons, it can form hexahydroxybenzene, while in the presence of Li^+ ions, it forms a Li salt. It has been shown that hexaketocyclohexane can yield 800 mAh/g (84% theoretical) in 0.3 M LiTFSI-[PY13][TFSI] electrolyte at 70 °C.[44] Li-rhodizonate, a compound from the same family of materials as hexahydroxybenzene, can deliver the practical capacity of 580 mAh/g (98% of theoretical 589 mAh/g) using 1 M $LiPF_6$ in ethylene carbonate and dimethyl carbonate (1:1 w/w) as an electrolyte.[45] However, as these are small molecules, they all have limited cycling stability due to dissolution in the electrolyte.

Aqueous electrolytes have several advantages over organic electrolytes: they are more environmentally friendly, have a higher ionic conductivity, and are non-flammable. The main disadvantage of aqueous electrolytes is the limited stability voltage window of water, which means a lower battery voltage and energy density. Theoretically, this means that aqueous batteries would be limited to an output voltage of only 1.23 V. In reality, we can achieve higher voltages of 2.1 V (overpotential) or even 3.2 V (additives) in lead-acid batteries,[46] but this is still lower than organic electrolytes, which can offer operating voltages of up to 5 V. One of the advantages of organic batteries is their compatibility with aqueous electrolytes. The redox potential of organic active materials is usually between 2–4 vs. Li/Li^+ or −1 V to 1 V vs. SHE, which means that they are mostly within the stability window of water. For this reason, several publications have recently been published on organic batteries with aqueous electrolytes (Table 1):

To obtain stable cycling, one approach is to prepare polymers that are not soluble in electrolyte. For that, we need to sacrifice at least one carbonyl/hydroxyl group on the benzene ring to enable connection within the polymer chain. The best candidate for this purpose is 1,2,3,4-tetrahydroxybenzene with a theoretical capacity of 755 mAh/g which can exchange four electrons. To the best of our knowledge, only two published works are showing 1,2,3,4-tetrahydroxybenzene electrochemistry: as grafted on carbon electrode[62] and as octahydroxytetraazapentacene (OHTAP).[63]

In this work, we first analyse 1,2,3,4-tetrahydroxybenzene as the best candidate among the different multi hydroxybenzene molecules and examine the possibility of polymerization. First, we show the electrochemical results of the model compounds in three redox states (MH4 - fully reduced, MH2 - partially reduced and M - oxidized). Based on these results, we can confirm the four-electron reaction of the proposed 1,2,3,4-tetrahydroxybenzene. Furthermore, we synthesize the insoluble polymer nanoparticles based on poly(2,3,4,5-tetrahydroxystyrene) or denoted as RPN 3c. We show that RPN 3c sample shows a similar CV as the model compound MH2: good electrochemical activity in acidic water-based electrolytes, but low activity in organic electrolytes with Li salt.

Table 1. Overview of Organic batteries using **Aqueous electrolytes**.

Classic batteries	Redox flow batteries
Active material is solid in electrode[47]	Active material in electrolyte
Zn-organic[18,21,52–54,22–24,26,48–51] All-organic[47,55–57] Organic-inorganic[47,58] Proton-organic[50,59]	issolved[60] Dispersed[61]

2. Results and Discussion

2.1. Analysis of Theoretical Capacity and Redox Behavior of Hydroxybenzene Molecules

The theoretical capacities of different hydroxybenzene molecules (Figure 1) were predicted by writing down the chemical structures of hydroxybenzenes in different redox states (Table S1 in Supporting info). For some redox states, we cannot write down suitable structures, which means that these states do not exist. Here are our conclusions:

- Electrons can be exchanged in pairs: 2, 4, or 6 electrons. The odd number of electrons leads to unstable radical species (phenol as an example).
- Only ortho and para positions allow reversible electron exchange.
- 1,2,4,5-Tetrahydroxybenzene is an exception to these rules. Although its hydroxyl groups are in para/ortho positions, the structure only allows an oxidation reaction with 2 electrons. This statement is supported by the literature reports on the capacities obtained with 1,2,4,5-tetrahydroxybenzenes and its derivatives. Table S2 shows various values of reversible capacity ranging from 42 to 99% of the theoretical capacity according to the 2-electron reaction.

2.2. Model Compounds

Model compounds prepared in three different oxidation states, i.e. MH4 (fully reduced model compound with four protons), MH2 (partially reduced model compound with two protons), and M (an oxidized model compound in a form of dihydrate) were used to prove four electron reaction for 1,2,3,4-tetrahydroxybenzene redox reaction (Figure 2a).

Model compounds were intentionally small molecules (monomers) to simplify the synthesis, purification, and characterization performed by NMR, IR, and high-resolution mass spectrometry. MH2 was prepared in a two-step reaction. Coenzyme Q_0 was alkylated using carboxylic acid ($C_{11}H_{23}$-COOH) with potassium persulfate ($K_2S_2O_8$)/silver nitrate ($AgNO_3$) (Figure 2b). In the next step, it was deprotected by boron tribromide (BBr_3) to obtain MH2. MH4 was synthesized by the reduction of MH2 with sodium dithionite. The oxidation of MH2 with 2,3-dichloro-5,6-dicyanobenzoquinone (DDQ) resulted in a

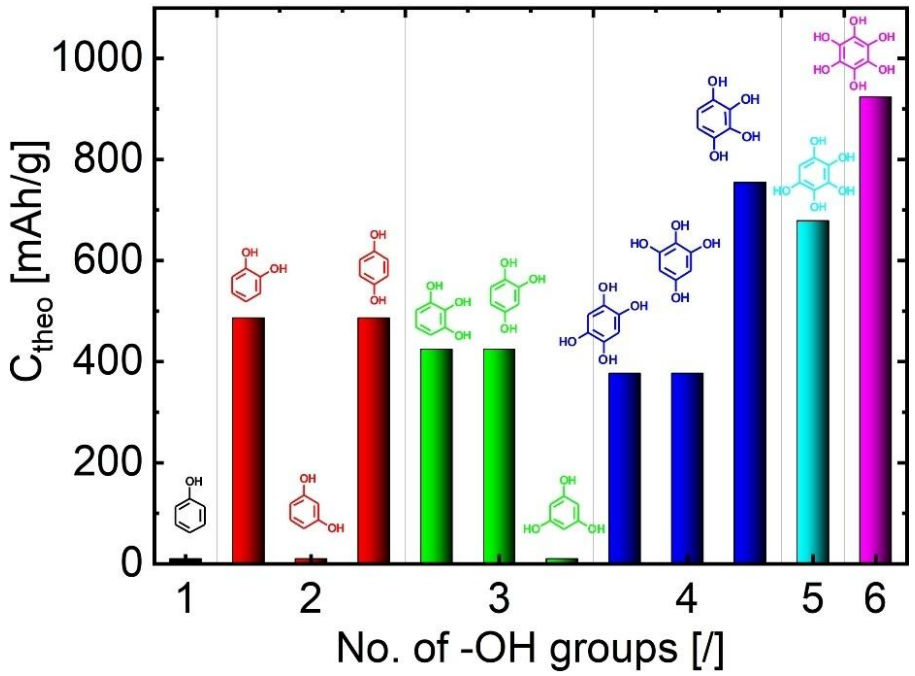

Figure 1. All hydroxybenzene isomers from 1 to 6 hydroxy groups and their predicted theoretical capacity. Predicted redox reactions are listed in supporting info in Table S1.

model compound M. More details about the synthesis and characterization of MH4, MH2, and M are in the Supporting info.

Initially, we measured cyclovoltammetry (CV) of the model MH2 compound in different electrolytes, based on 0.1 M LiTFSI salt (measurement details in Supporting info). Ten different solvents were tested (Figure 3a): acetonitrile (MeCN), dimethoxyethane (DME), 1,3-dioxolane (DOL), dimethyl carbonate (DMC), propylene carbonate (PC), gamma-butyrolactone (GBL), *N,N*-dimethylformamide (DMF), dimethyl sulfoxide (DMSO), methanol (MeOH) and water. Model compound MH2 showed broad peaks in organic electrolytes with a large separation between oxidation and reduction peaks. The best reversibility was obtained in aqueous electrolyte indicated by two oxidation peaks with the smallest separation (285 mV) and one sharp reduction peak. CVs in organic electrolytes were measured with Ag/Ag^+ reference electrode (~0.54 V vs. SHE) and potentials were adjusted by ferrocene standard (0.624 V vs. SHE).[64] Ferrocene corrections were collected inside Table S3, second column $E_{1/2}$ (Fc/Fc^+). CVs in aqueous electrolytes were measured with Ag/AgCl reference electrode with stable potential +0.203 V vs. SHE.[65] Results in aqueous electrolytes are shifted 421 mV to the left for better comparison with organic electrolytes.

Figure 3b shows the CVs of the selected compounds in acidic H^+ electrolytes. For aqueous electrolyte, 0.1 M $HClO_4$ was used. An anhydrous p-toluenesulfonic acid (PTSA) was used as a source of H^+ ions for organic electrolytes. PTSA was chosen because it is very acidic, dissolves well in organic solvents, and is stable within a certain electrochemical window. The change from the Li^+ to the H^+ system changed the electrochemistry of MH2 considerably:

- Redox peaks shifted to higher potentials which was already observed in the literature.[66,67]
- CV curves look more reversible, they have two oxidation and one reduction peaks with lower peak separation. We hypothesize the possibility that in Li^+ based organic electrolytes irreversible reactions occur, like insoluble salt formation Different stabilization of neutral and charged redox species has also a big influence on CV voltammograms. Better solvation can make some redox states more stable (lower energy). If the final state is stabilized more than initial one, then reaction becomes thermodynamically more favourable and reaction equlilibra shifts more to product. This can therefore affect the thermodynamics. Better solvation of the transition state means a lower activation energy and therefore a faster reaction. In this case, it affects the kinetics of the redox reaction.
- In some cases, the addition of water was necessary to maintain a stable CV (Figure S6). We observed that the addition of water in PTSA-based electrolytes with high resistance (Table S3), such as MeCN, DME, PC, and GBL (33.5 kΩ–67 kΩ), decreased the resistance after water addition (7.5 kΩ–10.1 kΩ). On the other hand, PTSA-based electrolytes with low resistance, such as DMF, DMSO and MeOH (1 kΩ–0.17 kΩ), worked well without traces of water.
- In a case of DOL, rapid exothermic polymerization of electrolyte occurred after addition of very acidic PTSA.
- In the case of DMC, even a 5% addition of water wasn't sufficient to get stable CV cycles and to get low resistance.

From the above results, we can conclude that the electrochemistry of MH2 with H^+ is better than with Li^+ based electrolytes. 0.1 M PTSA based electrolytes with sufficient

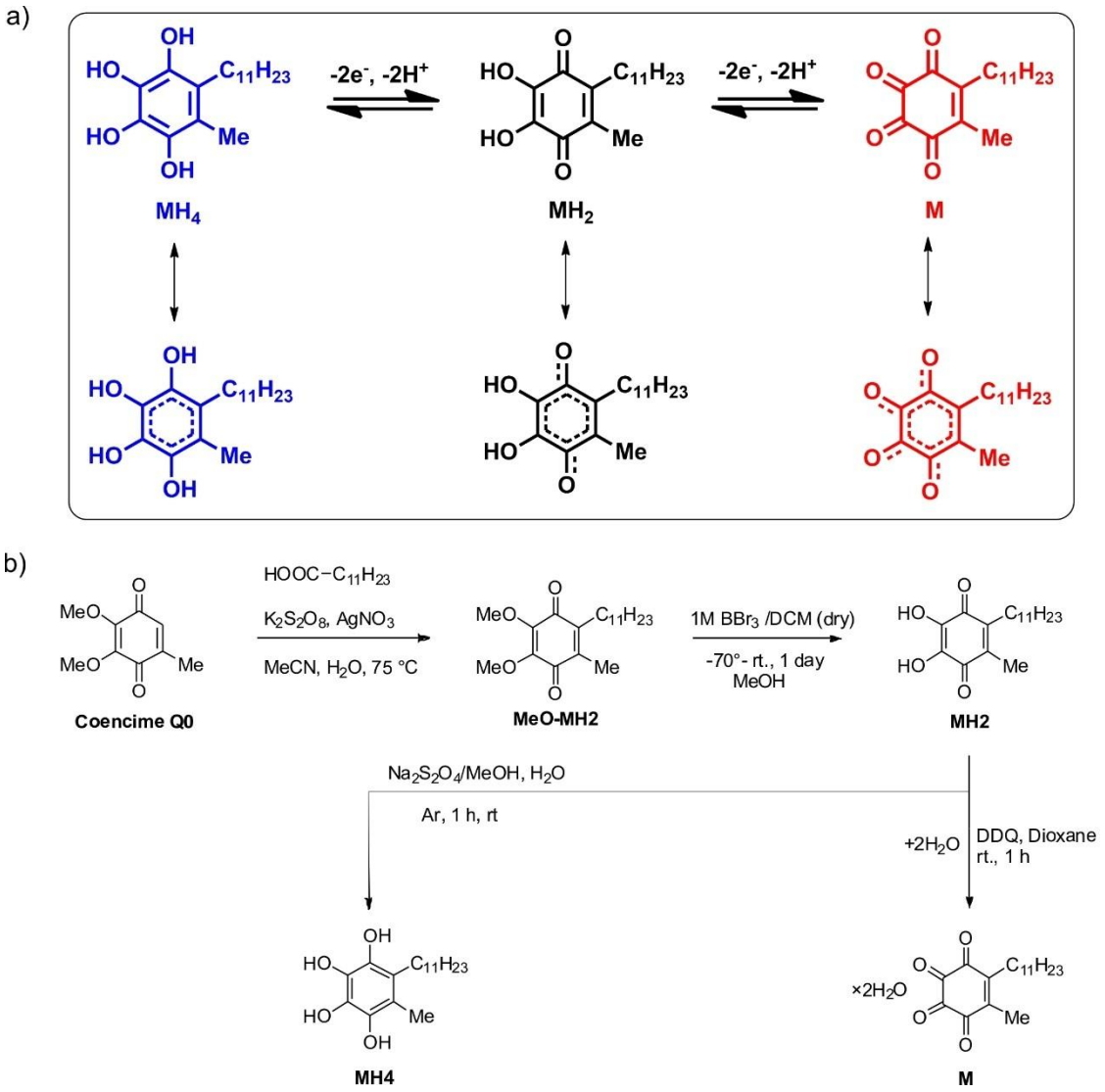

Figure 2. a) Scheme of four electron reactions from MH4 to M through intermediate MH2 in the presence of H^+ ion. b) Synthesis of model compounds MH2, M, and MH4.

conductivity (DMF, DMSO, and MeOH) work well without traces of water. In other cases, water is added to the organic electrolytes to lower their resistance and enable a stable CV measurement.

In all previous examples, we have seen two oxidation peaks and only one reduction peak for the model compound MH2. According to the reversible redox reaction, we would expect two reduction peaks. Indeed, at very fast scan rates (40 V/s and 5 V/s), we observed two reduction peaks when 0.1 M PTSA in DMF electrolyte was used (Figure 4a). According to these results, the reaction is reversible at very fast scan rates and then gradually becomes quasi-reversible at lower rates. Another explanation is that redox reaction MH4- > MH2 - > M:

At slow rates 200 mV/s: All MH2 is oxidized to M. Then M is reduced to MH4 in one step. Thus we see only one reduction peak at −0.5 V vs. Fc/Fc^+.

At fast rates 40 V/s: MH2 is only partially oxidized to M. If we compare surfaces under the peaks, we can confirm that the ratio S2/S1 really decreases from 1.63 to 0.49 when we change from slow to fast scan rate (Figure 4b and 4c). During reduction we can see two reduction peaks (0.3 V and −0.5 V vs. Fc/Fc^+). First peak corresponds reduction of MH2 to MH4, and the second one M to MH4.

We then compared the CV of MH2 in LiTFSI and $HClO_4$ aqueous electrolytes at a scan rate of 10 mV/s (Figure S1). In the neutral LiTFSI electrolyte, the reduction peak at −0.526 V vs. Ag/AgCl shrinks and shifts to lower values with cycling (Figure S1a). The oxidation peaks at −0.144 V and 0.117 V vs. Ag/AgCl almost disappear by the 25th cycle. This indicates the irreversible reactions that take place during reduction and oxidation. On the other hand, compound MH2 in acidic 0.1 M $HClO_4$ electrolyte shows a quasi-reversible redox reaction with two oxidation peaks at 0.119 and 0.404 V vs. Ag/AgCl and one reduction peak at −0.399 V vs. Ag/AgCl (Figure S1b). A small

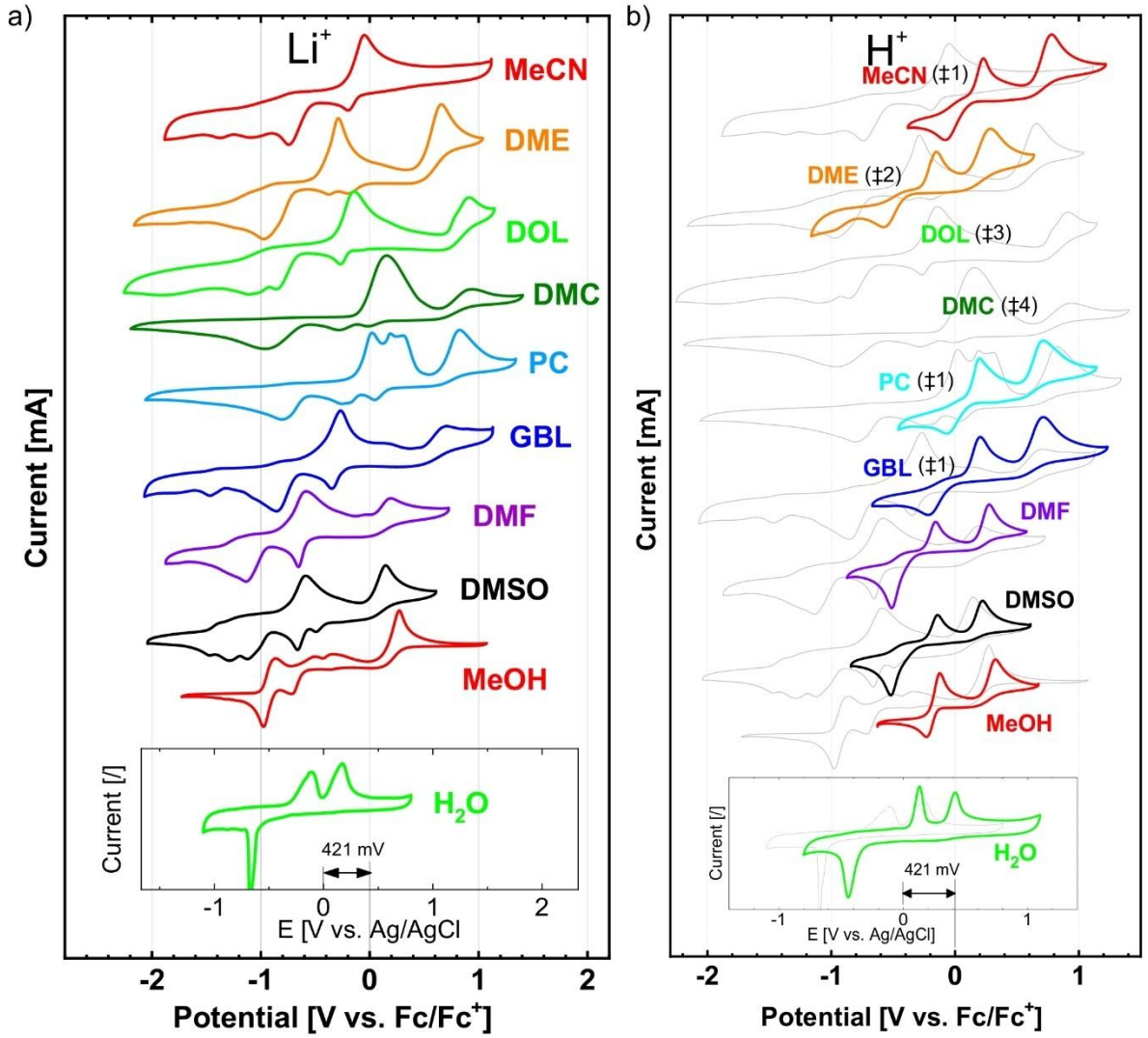

Figure 3. CVs of model compound MH2 in a) 0.1 M LiTFSI based organic electrolytes vs. ferrocene reference. The inset shows CVs of aqueous electrolyte vs. Ag/AgCl reference. b) 0.1 M PTSA based organic electrolytes and 0.1 M $HClO_4$ based aqueous electrolyte. In some cases: (‡1) MeCN, PC, GBL 0.18 wt. % water or (‡2) DME 5 wt. % of water addition was needed to get stable CV. In some cases we were not able to get stable CVs: (‡3) DOL polymerization and (‡4) DMC 5 wt. % water not enough for stable CV. All CVs were measured at a scan rate of 50 mV/s.

shift in the peaks is present here, but it is probably just an increase in resistance due to adsorption on the working electrode. In the literature, we find similar behaviour with catechols which only undergo reversible redox reactions in acidic media (pH < 4). Under neutral or basic conditions, irreversible redox peaks appear in the CV of catechols which is explained by complicated side reactions of the reactive radical anion with catechol or electrolyte.[68–70] All CV measurements in 0.1 M LiTFSI (pH = 6.8) and 0.1 M $HClO_4$ (pH = 1.0) were measured within the stability window at the glassy carbon electrode (GC). For 0.1 M LiTFSI, the measured stability window was between −1.3 V (H_2 evolution) and 1.1 V versus Ag/AgCl (O_2 evolution). At 0.1 M $HClO_4$, the measured lower stability potential (H_2 evolution) fluctuated strongly between −1.1 and −0.6 V vs. Ag/AgCl during the experiments. The high-voltage stability potential (O_2 evolution) in 0.1 M $HClO_4$ was 1.3 V vs. Ag/AgCl. Our measured stability values for the GC electrode are similar to those reported in the literature[71] and may vary depending on the electrode cleaning procedure, pre-treatment, electrolyte, etc.[72–76]

After the successful chemical synthesis of MH4, MH2, and M, we investigated whether they could be synthesized electrochemically from one to another. For this reason, we measured the CVs of the other two model compounds M and MH4 in an aqueous 0.1 M $HClO_4$ electrolyte (Figure 5a). In the first scan of the model compound M, there is no oxidation peak at ~0.4 V vs. Ag/AgCl as the compound is already oxidized. During reduction, a peak at −0.361 V with a shoulder at −0.440 V is observed followed by oxidation at 0.136 V vs. Ag/AgCl. In the following cycles, the CV curve of M is similar to MH2 with some differences. The reduction peak at −0.361 V is converted into −0.482 V. In addition, a small oxidation peak at 0.248 V and a reduction peak at 0.129 V appear during cycling. We are still investigating appearance of this small peak and possible

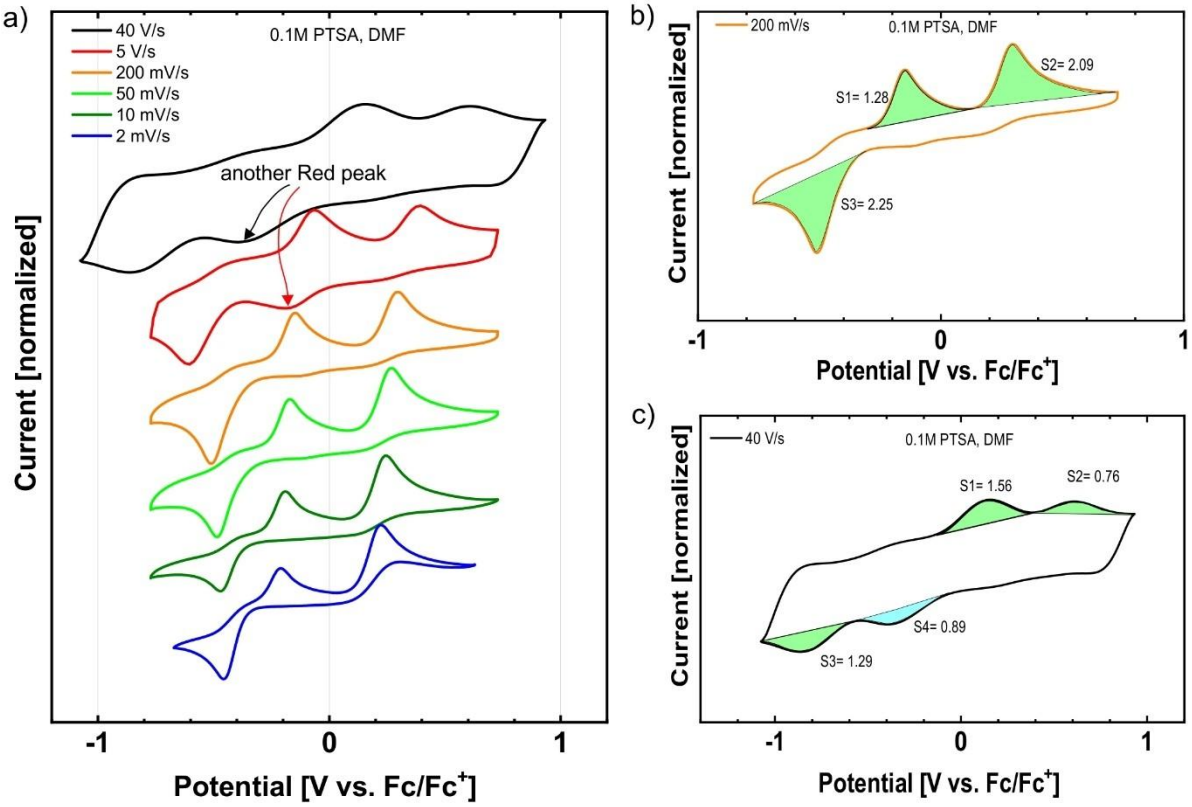

Figure 4. a) CV of the model compound MH2 at different scan rates in 0.1 M PTSA in DMF electrolyte. At high scan rates, we can observe another reduction peak. CV at b) 200 mV/s and c) 40 V/s. Surface areas of peaks were integrated and their values are written beside.

explanation could be a side reaction: formation of dimerization product (dioxin) which was also mentioned in the literature.[77–79]

CV of the reduced compound MH4 is shown in Figure 5b. Similar to the other two model compounds, MH4 exhibits one reduction and two oxidation peaks. We observed some degradation in the first scan, which can be observed as an irreversible oxidation reaction with an unstable potential above 0.5 V. In the next cycles, the third oxidation peak appears at 0.615 V, which gradually disappears by the 10th cycle. The CV curve of MH4 strongly resembles that of MH2 in later cycles.

We have found CV of MH4 rather confusing. This experiment was performed in a three electrode beaker cell, where a small amount of MH4 (less than 0.1 mM) was dissolved in 0.1 M $HClO_4$ electrolyte, and working electrode (WE) was a glassy carbon. In this setup even small amounts of oxygen can interfere and can cause additional peaks. Additionally since we are dealing with multi-electron processes coupled with chemical reactions, the exact redox mechanism is much more complex than this simplified reaction M MH2 MH4. These additional minor peaks could be secondary reactions between reduced MH2 or MH4 formed on the electrode surface and M in the bulk electrolyte and are difficult to explain. Another problem can be also different adsorption of redox active species on WE during CV experiment: some can adsorb stronger and can result in much stronger CV curve, even if their concentration in electrolyte is negligible.

To avoid most of these problems, MH4 was mixed with conductive carbon and PVDF binder, and coated on the glassy carbon electrode (WE). With this setup we have avoided secondary reactions in vicinity of electrode and different adsorption. Figure below (Figure 5c) shows CV response of MH4 on electrode where we don't notice appearance additional oxidation peaks.

Figure 6 compares the electrochemical response for all three model compounds M, MH2 and MH4. The electrochemical behaviour is similar and the majority of the electrochemical activity for all three compounds measured is based on two oxidation peaks at ~0.13 V and ~0.42 V and a reduction peak at ~−0.43 V vs Ag/AgCl. The observed similarities indicate that all three compounds can be electrochemically converted into another. Considering that the change of oxidation state from MH to MH4 requires 4 electrons, we have indirect evidence that 1,2,3,4-hydroxy benzene or its oxidized forms can quasi-reversibly exchange 4 electrons and could therefore be a promising redox centre for future high-energy organic batteries. The four-electron redox reaction has been demonstrated in acidic aqueous media and could therefore be used for proton batteries.

We have conducted two more experiments to indirectly confirm four different redox reactions (Figure 6b, reactions 1)–4)):

1) **Limiting cut-off potential**: If we limit oxidation potential to 0.3 V vs. Ag/AgCl, only reduction 4) and no 3) is observed.

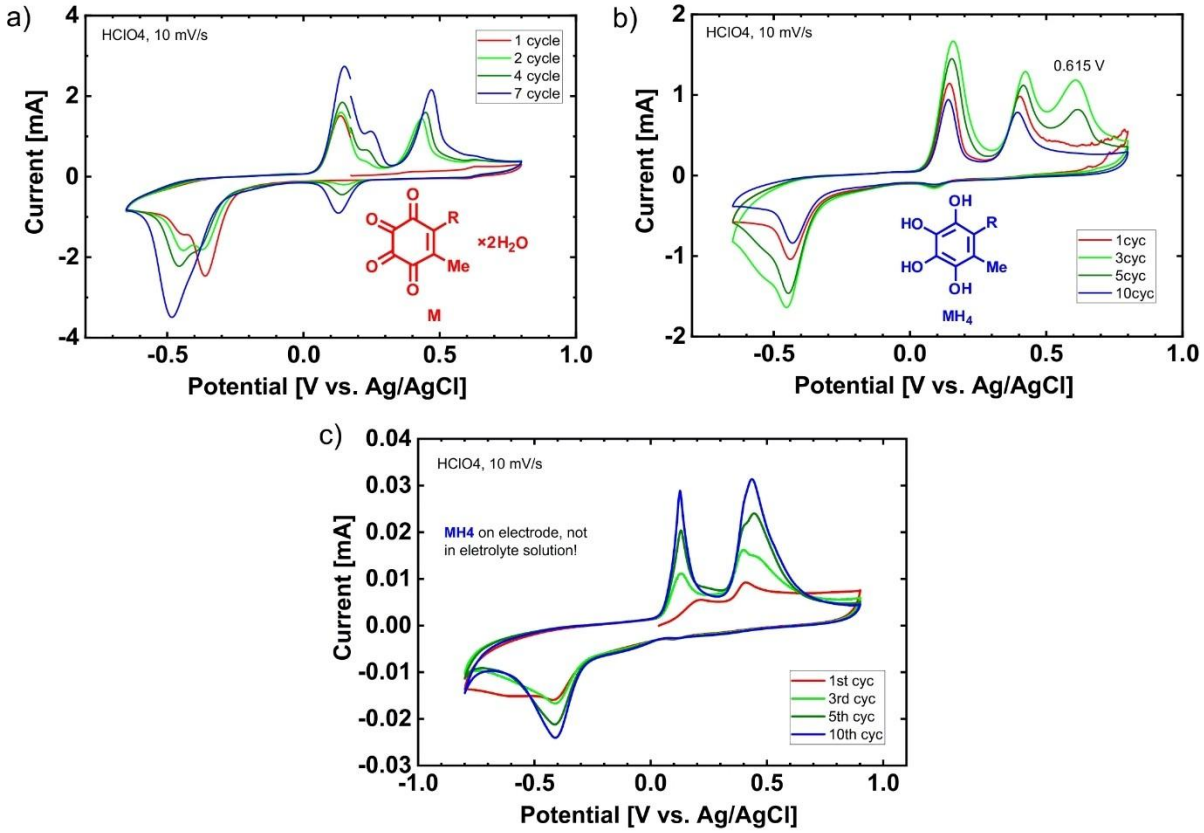

Figure 5. CV of a) oxidized compound M and b) reduced MH4 compound, dissolved in aqueous 0.1 M $HClO_4$ at 10 mV/s. c) MH4 was applied directly on working electrode (not in solution).

2) **Protected derivative MeO-MH2**: As–OMe groups are electrochemically inactive, only MeO-MH2/MeO-MH4 redox reaction is possible. This is in agreement with CV, where we can only observe one oxidation 1') without oxidation 2) and one reduction 4'). As MeO-MH2 is closely related to MH2 also E1/2 redox potentials are very similar 112 mV and 208 mV vs. Ag/AgCl.

2.3. Polymer Poly(2,3,4,5-tetrahydroxystyrene)

The model compounds MH2, MH4 and M have a high solubility and cannot be used for electrodes with a high solids content. For this reason, we have developed Redox-active Polymer Nanoparticles based on 99 wt% poly(2,3,4,5-tetrahydroxystyrene) cross-linked with 1 wt% divinylbenzene, with the abbreviation RPN 3c (Figure 7 and Figure 8a). The crosslinking was used to prevent the solubility of the polymer and to improve cycling stability. We have additionally measured solubility of RPN 3c and MH2 in five electrolytes (Table S4). We can see that polymer RPN3 was insoluble ($<$1 mg/mL) in all measured electrolytes. Monomeric MH2 was insoluble only in aqueous electrolyte, but soluble organic electrolytes (13–200 mg/mL).

The linear polymer 2c was prepared by emulsion polymerization of the monomer 2,3,4,5-tetramethoxystyrene (1a). The copolymer RPN 2c was prepared by crosslinking with 1 wt.% divinylbenzene. The second step was deprotection with BBr3, resulting in linear 3c or crosslinked RPN 3c. The linear polymer 3c was mainly used for characterization and the cross-linked RPN 3c was used for battery applications due to its insolubility. The polymers were characterized by IR spectroscopy, GPC, NMR, IR, TGA, DSC, SEM and DLS (see Figures S2–S5). The synthesis approach was adopted from the recent report on the synthesis of polycatechol nanoparticles.[80]

The particle size of active material is an important factor in Li batteries. Short diffusion paths for Li^+ ions in small particles and particles that are electronically well-contacted with the current collector are required for the optimal operation of the battery. To reach this goal we used the emulsion polymerization technique which resulted in very small 40 nm-sized nanoparticles RPN 3c as was demonstrated by SEM images (Figure 8a and Figure S5). Another important factor is the swelling of polymers inside electrolyte. In this way electrolyte can directly penetrate between polymer chains and greatly enhance ion transport – as it was shown recently.[14]

Due to the insolubility of RPN 3c, we moved from solution electrochemistry to electrodes where a thin layer of RPN 3c, mixed with conductive carbon and PVDF binder was coated on the glassy carbon discs (see Supporting info). The electrochemical characterization of RPN 3c was performed in three different electrolytes: 0.1 M $HClO_4$ in water, 0.1 M LiTFSI in water, and 0.1 M LiTFSI in acetonitrile using CV at a scan rate of

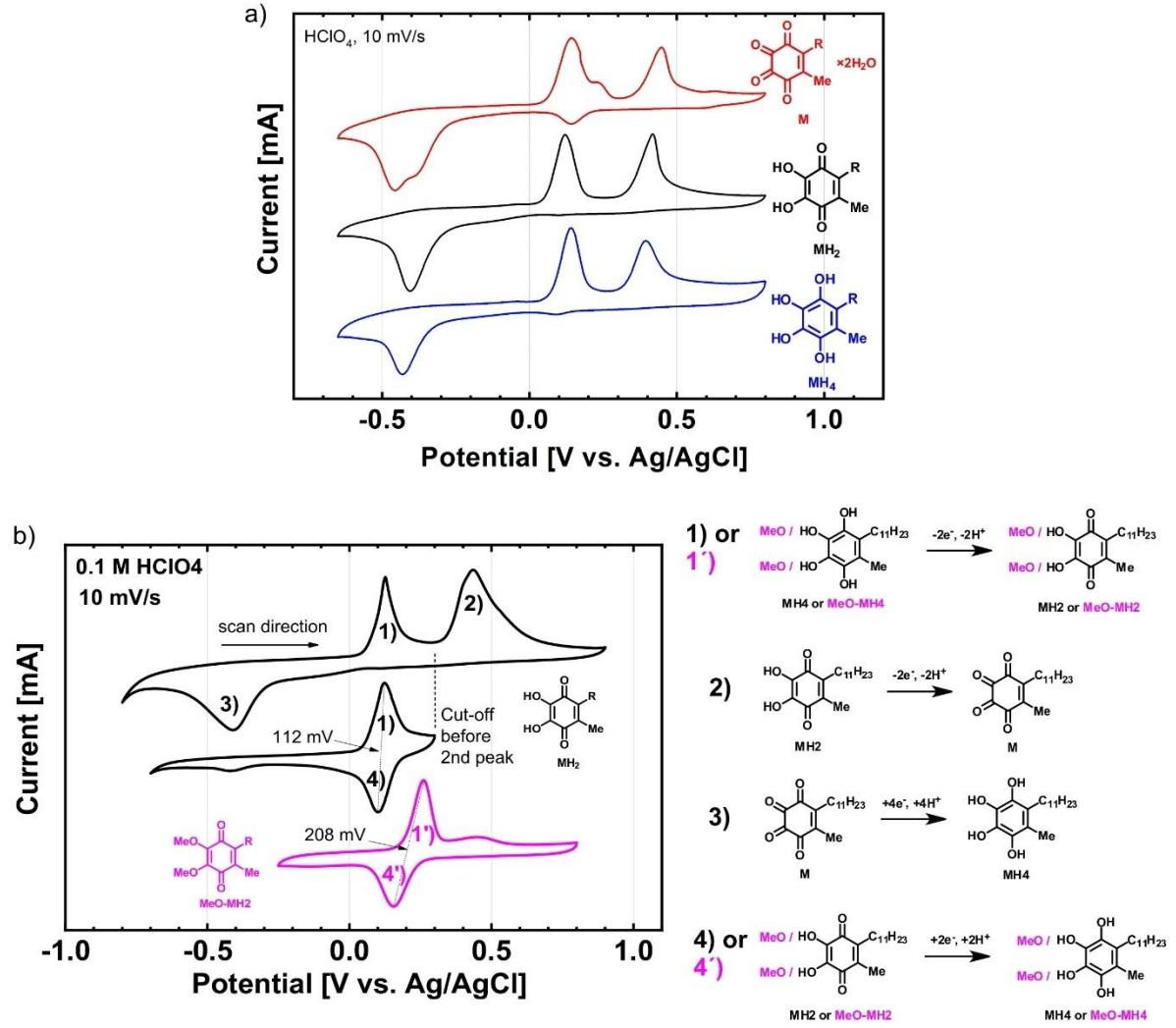

Figure 6. CV curves for all three compounds M, MH2, and MH4 in 0.1 M $HClO_4$ at 10 mV/s, 10th cycle in all cases. b) CV of MH4 (black) and MeO-MH2 (magenta) model compounds at scan rate 10 mV/s and 0.1 M $HClO_4$ electrolyte. On the right, there are proposed redox reactions for each redox peak from 1) to 4).

Figure 7. Two-step reaction scheme to obtain redox-active polymer 3c and crosslinked nanoparticles RPN 3c.

10 mV/s (Figure 8b). The acidic aqueous electrolyte shows the highest electrochemical activity. In this electrolyte, the redox peaks are well separated and shifted to higher potentials compared to the aqueous 0.1 M LiTFSI electrolyte. The electrochemical characterization of 0.1 M LiTFSI in an acetonitrile-based electrolyte shows a low redox activity. The results obtained with the RPN 3 C polymer are consistent with the observations made with the model compound MH2.

Figure 8c compares the CV responses of the RPN 3c polymer and the model compound MH2 in an aqueous 0.1 M $HClO_4$ electrolyte at a scan rate of 10 mV/s, measured in the three-electrode cell. We can see that the CV shapes for both materials

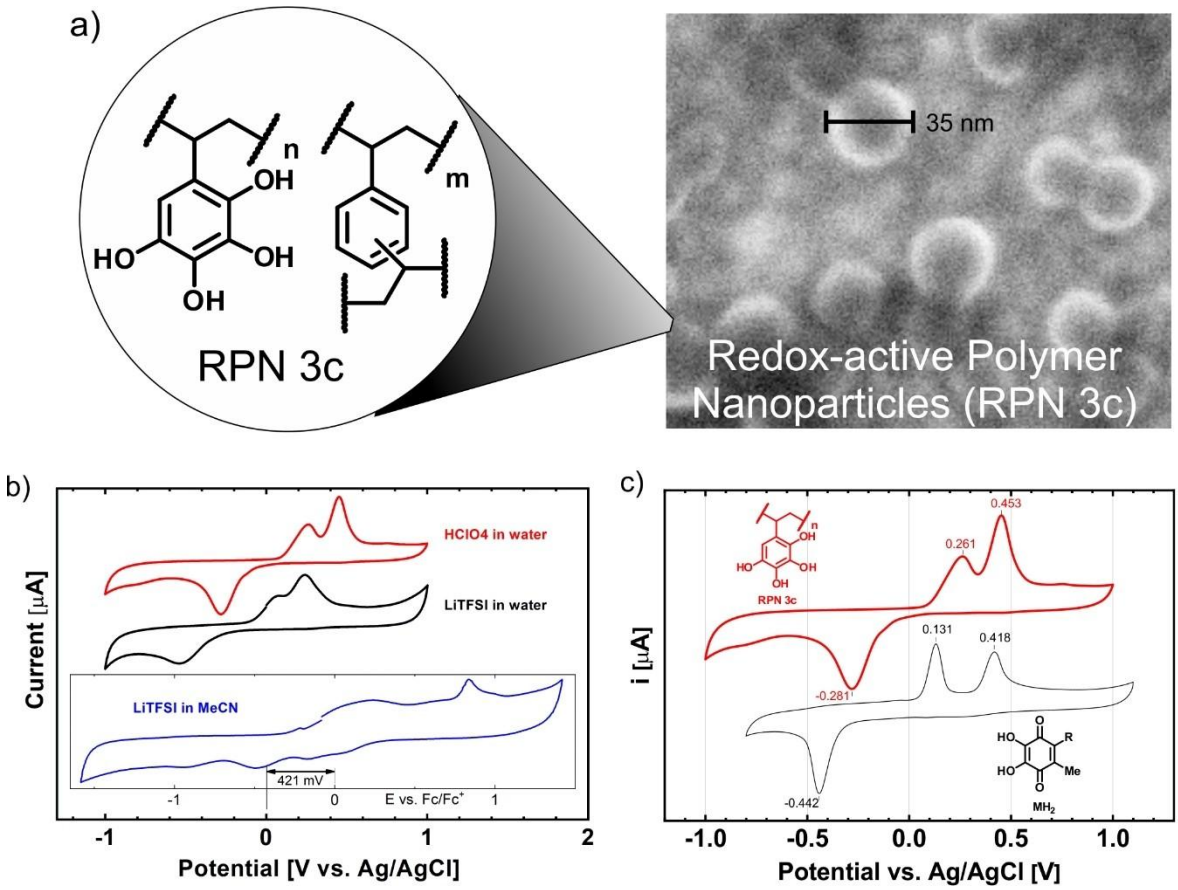

Figure 8. a) Chemical structure of Redox-active polymer nanoparticles (RPN 3c) and SEM image of polymerized nanoparticles, b) CV of RPN 3c in two aqueous electrolytes and acetonitrile (MeCN) at 10 mV/s. In acetonitrile graph is shifted 421 mV due to different reference electrodes, c) CV of RPN 3c and model compound MH2 in 0.1 M $HClO_4$ in water at 10 mV/s.

are very close to each other, with two oxidation peaks and one reduction peak. The peaks of RPN 3c (0.261, 0.453, and −0.281 V vs. Ag/AgCl) are shifted to higher potentials, which can be explained by the absence of the electron-donating methyl group present in MH2. Electron-donating groups increase the energy of the LUMO orbital and thus lower its redox potential.[81–84]

Finally, the electrochemical activity of RPN 3c polymer was checked in Li-battery. Two different binders were used for the preparation of RPN 3c electrodes: poly(tetrafluoroethylene) or PTFE and poly(vinylidene fluoride) or PVDF with the latter showing a better performance (Figure S7). The RPN 3c polymer was used as the positive electrode and it was coupled with metallic lithium as the negative electrode. The electrochemical characteristics were tested in three different electrolytes 1 M LiTFSI-based electrolytes: 1,3-dioxolane + 1,2-dimethoxyethane (DOL + DME), gamma-butyrolactone (GBL), and propylene carbonate (PC). The obtained results were compared with the electrochemical activity of RPN 3c polymer in 1 M $LiPF_6$ in ethylene carbonate + diethyl carbonate (EC + DEC) electrolyte. More details are given in the SI file. The best specific capacities were obtained in the DOL + DME electrolyte. The material can deliver a specific capacity of 111 mAh/g in the second cycle. The capacity drops to 34 mAh/g after 50 cycles (Figure 9a). Initial capacities of 55, 48 and 37 mAh/g were achieved in GBL, EC + DEC and PC electrolytes, respectively, dropping to around 27–22 mAh/g after 50 cycles (Figure 9a). Even the highest measured specific capacity of 111 mAh/g corresponds to only 18% of the theoretical capacity (631 mAh/g for RPN 3c material). This low capacity can be explained by the low electrochemical activity in organic electrolytes, as already observed for the model compound MH2.

The Coulombic efficiency (CE) was calculated as the ratio between the capacity obtained during the reduction and oxidation processes, which was above 100% for all tested electrolytes in the first cycle. This is most likely related to additional irreversible reactions in the first (formation) cycle. Thereafter, CE stabilizes between 97 and 100% for the electrolytes EC + DEC, GBL and PC. For the DOL + DME electrolyte, the Coulombic efficiency dropped to 61% in the 5th cycle and then slowly stabilized at 90–92% after 25 cycles. The reason for this low efficiency is the low oxidation stability of this electrolyte above 3.5 V compared to Li/Li+. Cycling in the narrow voltage window between 1.5 and 3.5 V vs. Li/Li+ enables a Coulomb efficiency of almost 100, but the capacity achieved is only 65 mAh/g (Figure S8).

The additional information that can be derived from the galvanostatic curves is a differentiation between redox activity

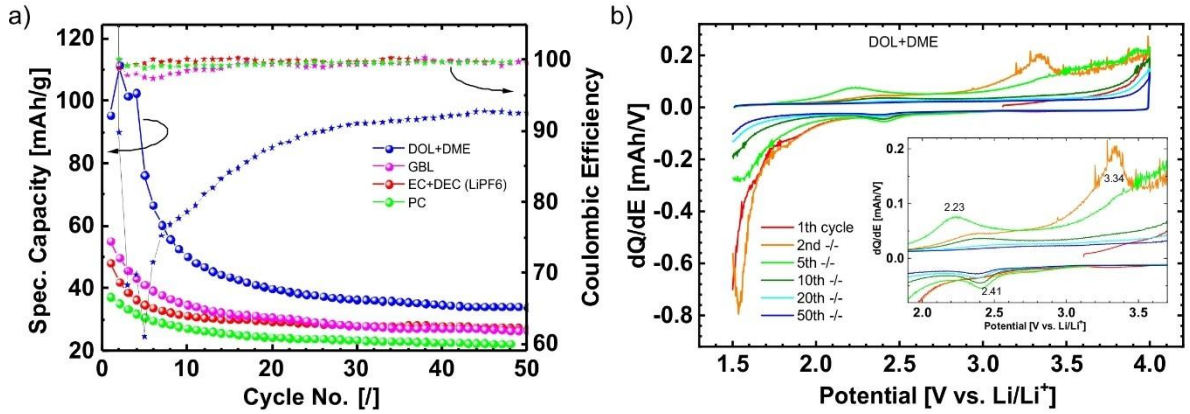

Figure 9. Electrochemical testing of RPN 3c in Li battery: a) Cycling of RPN 3c in four different electrolytes at 50 mA/g, potential window 4.0–1.5 V vs. Li/Li^+ b) derivative dQ/dE curves in DOL + DME based electrolyte. The inset graph is a zoomed region with some redox activity visible in the first few cycles. In all cases, PVDF electrodes were used.

and pseudocapacitance which can be observed from the derivative curves dQ/dE (Figure 9b and Figure S9). For instance, in 2nd cycle, we can see an oxidation peak at 3.3 V and small reduction peaks at 2.3–2.5 V in all tested electrolytes. In DOL + DME oxidation peak at 2.23 V is visible in the 5th cycle (Figure 9b). In other electrolytes oxidation peaks at 2.66–2.78 V and reduction peaks at 3.14–3.18 V could be observed (Figure S9). All these peaks disappear during cycling leaving an almost flat curve after 50 cycles. These observations indicate there is redox activity in the starting cycles which is lost in the first 50 cycles. After 50 cycles remaining capacity is mostly attributed to the pseudo-capacitive behavior of carbon black.

The low electrochemical performance of the RPN 3c cathode in a Li battery is related to the fact that the non-protic electrolytes can be combined with metallic lithium. Therefore, we decided to test the model compound MH2 and RPN 3c in a Zn battery where the electrolyte is a slightly acidic aqueous solution of $ZnSO_4$ (pH = 4.7). We first performed CV to determine the potentials of the redox peaks and the electrochemical stability window, followed by galvanostatic cycling to determine the capacity stability. Similar to the Li battery system, the electrodes with PVdF binder performed better than those made of PTFE (Figure S10, in SI). Further characterization with cyclic voltammetry shows that the MH2 cathode in the Zn battery has two oxidation peaks at 1.33 V and 1.50 V vs. Zn/Zn^{2+} and two reduction peaks at 0.76 V and 0.39 V vs. Zn/Zn^{2+}. There are also two minor reduction peaks at 0.99 V and 0.57 V vs. Zn/Zn^{2+} (Figure 10a and 10b). In the 2nd cycle, four oxidation peaks appear at 1.10 V, 1.25 V, 1.38 V, and 1.55 V as well as four reduction peaks (two of which are minor). The intensity of the peaks decreases rapidly with the cycles and after 10 cycles we can usually only see a flat pseudo-capacitive CV curve.

The CV of the polymer RPN 3c has a large oxidation peak at 1.47 V against Zn/Zn^{2+} and two small reduction peaks at 0.80 V and 0.42 V (Figure 10c and 10d). The intensity of the peaks decreases in the following ten cycles. The oxidation peak shifts downwards to 1.16 V against Zn/Zn^{2+}. Two reduction peaks are replaced by a peak at a higher potential of 1.10 V.

The electrochemical characterization of the MH2 sample in the galvanostatic cycling modes shows a long plateau at 1.20 V and one at 1.54 V vs. Zn/Zn^{2+} (Figure 11a) during the first oxidation (charge). During the first discharge, two plateaus at 0.80 V and 0.43 V are obtained. In later cycles, we have two charge plateaus at 1.10 and 1.45 V vs. Zn/Zn^{2+}. During discharge, we have two plateaus at 0.73 V and 0.41 V vs. Zn/Zn^{2+} (Figure 11b). Similar to CV results redox plateaus quickly disappear with cycles and after 30 cycles the electrochemical curve resembles the pseudo-capacitive behavior.

During charge, RPN 3c has a long plateau at a potential 1.38 V vs. Zn/Zn^{2+} (Figure 11c). Later charging cycles show no visible plateaus and are more inclined with an average of 1.33 V vs. Zn/Zn^{2+}. But at the 30th cycle charge plateau at 1.15 V becomes apparent. During discharge, there are no specific plateaus and the average potential is 0.63 V.

If we compare the cycling of the two materials, we can see that MH2 has a high initial capacity of 118 mAh/g which drops sharply to 12 mAh/g after 10 cycles and then a slow drop to 10 mAh/g after 26 cycles (Figure 11d). RPN 3c, on the other hand, has initial capacity 52 mAh/g and a more steady drop to 19 mAh/g after 10 cycles and to 14 mAh/g after 30 cycles. The Coulombic efficiency of MH2 is only 32% in the first cycle due to the very large charge plateau. It then rises rapidly to 95% after 10 cycles. In later cycles, it slowly stabilizes at around 97%. The polymer RPN 3c has 95% in the first cycle, then falls to 79% in the next two cycles. Later it gradually increases to 91% in 12 cycles and then to 94.4% in 26 cycles. It is unclear why MH2 has a higher efficiency than RPN 3c after the 3th cycle. However, we have to keep in mind that cycling window 0.3 to 1.6 V vs. Zn/Zn^{2+} is already outside the theoretical stability of water: H_2 evolution should be in theory at 0.48 vs. Zn/Zn^{2+} (pH = 4.7, $E_{H(pH=4.7)} = -0.28$ V vs SHE) and O_2 evolution should be at 1.71 vs. Zn/Zn^{2+} (pH = 4.7, $_{EO(pH=4.7)} = 0.95$ vs. SHE). It is possible that RPN 3c is more catalyzing O_2 evolution and/or less H_2 evolution than MH2 and thus oxidation (charging) is slightly extended and the efficiency is lower.

From the above results, we can conclude that both MH2 and the polymer RPN 3c were electrochemically active in the Zn

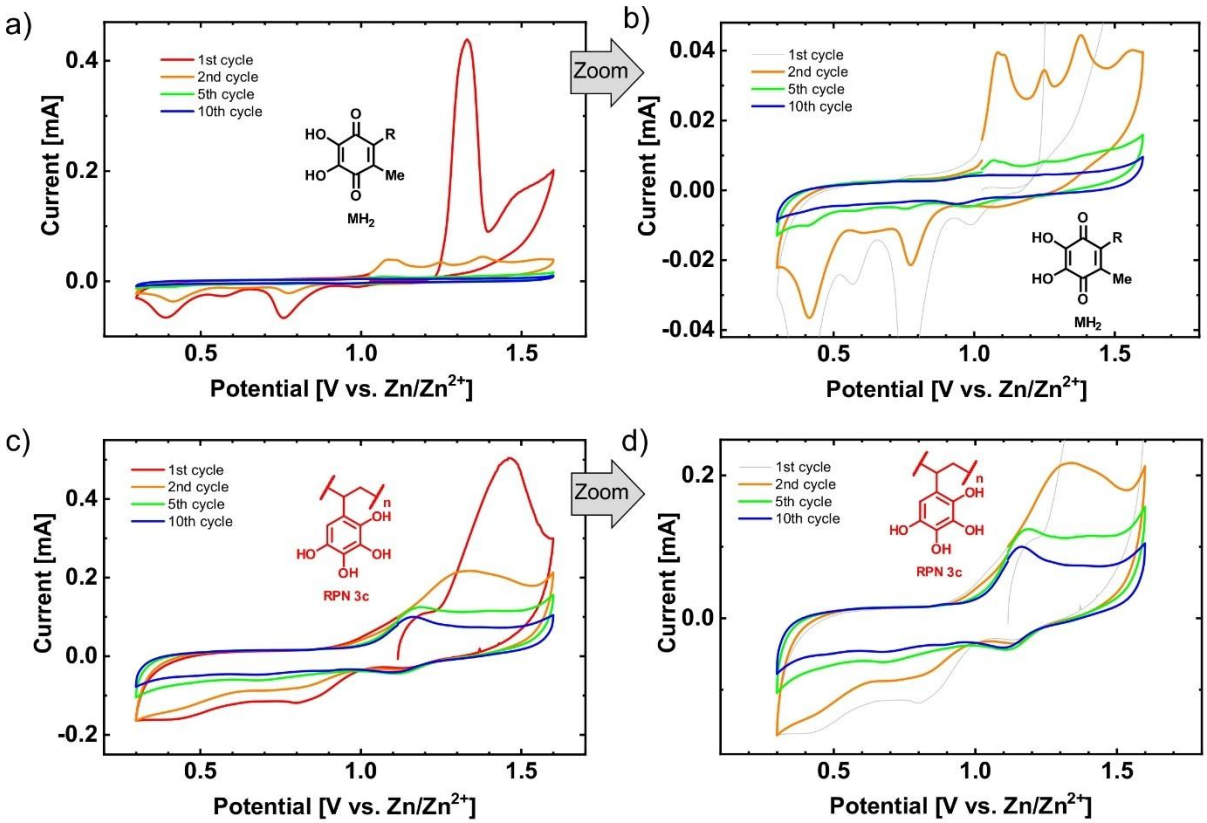

Figure 10. CV of Zn-organic battery at a scan rate 0.1 mV/s: a) and b) compound MH2, c) and d) polymer RPN 3c were used as positive electrode materials. In all cases, PVDF electrodes were used.

battery. It seems that the polymerization somehow improved the cycling stability, but on the other hand, worsened the utilization of the material – probably due to the limited ionic and/or electronic transport within the RPN 3c polymer.

3. Conclusions

In this work, we propose 1,2,3,4-tetrahydroxybenzene as a suitable candidate from the family of hydroxybenzene or polyphenol compounds. To test the electrochemical activity and stability, we prepared three model compounds: MH4, MH2, a partially oxidized MH4, and M, a fully oxidized MH4. All three model compounds showed similar CV signals with one reduction and two oxidation peaks in 0.1 M HClO4 electrolyte. This result supports our hypothesis of a quasi-reversible 4-electron exchange. The electrochemical performance of MH2 was better in proton-containing electrolytes than in lithium-containing ones. In organic electrolytes, PTSA was successfully used as a proton source: DMF, DMSO and MeOH worked well with anhydrous PTSA and other solvents required traces of water.

In the second part, we prepared insoluble redox-active polymer nanoparticles RPN 3c, based on poly(2,3,4,5-tetrahydroxystyrene), which can be used as active material in the battery. The electrochemistry of these nanoparticles is very similar to the electrochemistry of the model compound MH2 observed in a water-based electrolyte with 0.1 M $HClO_4$ salt. The polymer was tested in a lithium battery with four different organic electrolytes, but the electroactivity in the tested environments was very low.

MH2 and RPN 3c were tested in a Zn battery using a slightly acidic aqueous solution. Both materials showed reversible electrochemistry. As expected, the RPN 3c polymer was more stable than MH2. However, the initial capacity of 52 mAh/g is only 8% of the theoretical 631 mAh/g.

Through designed experiments with different modeled compounds tested in different electrolytes, we confirmed the four-electron exchange reaction. The low utilization of the polymer could be improved in the future by optimizing the chemical structure (copolymers) and optimizing the electrodes.

Acknowledgements

This work was financially supported by the European Research Council by Starting Grant Innovative Polymers for Energy Storage (iPes) 30625 and Slovenian Research Agency under research projects J2-8167, N2-0214 and N2-0165, research program P2-0423, public call MS-ERC-FS/2017- 002, Ministry of Education, Science and Sport (MIZS) for funding M.Era-net project InsBioration (call 2021) and Honda R&D Germany.

N.B. acknowledges the financial support obtained through the Post-Doctoral fellowship Juan de la Cierva-Incorporación

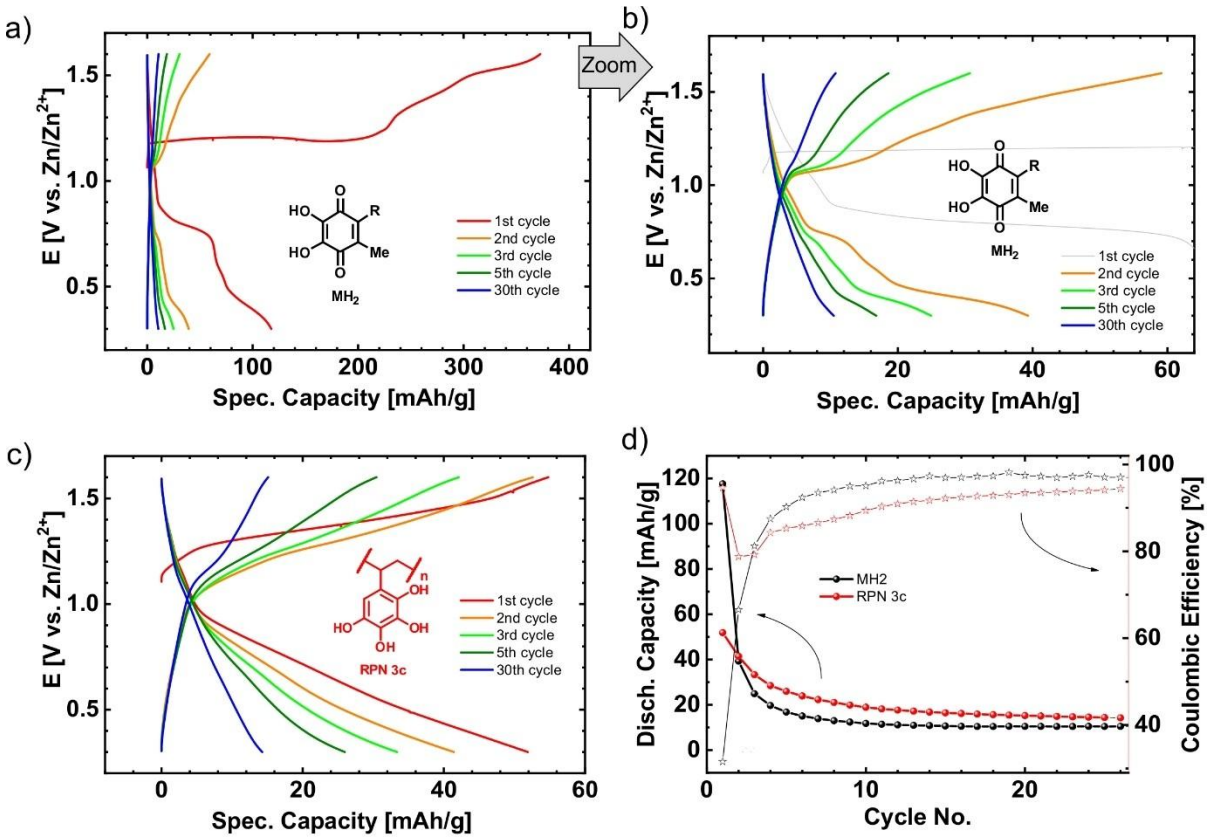

Figure 11. Galvanostatic cycling of Zn-organic battery at 50 mA/g, 1.6–0.3 V vs. Zn/Zn^{2+}: a) and b) positive electrode was MH2, c) positive electrode was polymer RPN 3c, and d) cycling stability of MH2 and RPN 3c. In all cases, PVDF electrodes were used.

(IJCI-2016-28442), from the Ministry of Economy and Competitiveness of Spain.

Conflict of Interests

The authors declare no conflict of interest.

Data Availability Statement

The data that support the findings of this study are available from the corresponding author upon reasonable request.

Keywords: Organic cathodes · polyphenols · Catechols · Li-organic battery · Zn-organic aqueous battery

[1] Q. Zhao, Y. Lu, J. Chen, *Adv. Energy Mater.* **2017**, *7*, 1601792.
[2] Z. Jian, Y. Liang, I. A. R. Pérez, Y. Yao, X. Ji, *Electrochem. Commun.* **2016**, *71*, 5–8.
[3] A. Ponrouch, J. Bitenc, R. Dominko, N. Lindahl, P. Johansson, M. R. Palacin, *Energy Storage Mater.* **2019**, *20*, 253–262.
[4] C. Ding, C. Li, H. Tian, Y. Tong, W. Huang, Q. Zhang, *Batteries & Supercaps* **2022**, *5*, e202200160.
[5] J. Bitenc, K. Pirnat, T. Bančič, M. Gaberšček, B. Genorio, A. Randon-Vitanova, R. Dominko, *ChemSusChem* **2015**, *8*, 4128–4132.
[6] J. Bitenc, K. Pirnat, G. Mali, B. Novosel, A. Randon Vitanova, R. Dominko, *Electrochem. Commun.* **2016**, *69*, 1–5.
[7] B. Pan, J. Huang, Z. Feng, L. Zeng, M. He, L. Zhang, J. T. Vaughey, M. J. Bedzyk, P. Fenter, Z. Zhang, et al., *Adv. Energy Mater.* **2016**, *6*, 1600140.
[8] B. Pan, D. Zhou, J. Huang, L. Zhang, A. K. Burrell, J. T. Vaughey, Z. Zhang, C. Liao, *J. Electrochem. Soc.* **2016**, *163*, A580–A583.
[9] J. Tian, D. Cao, X. Zhou, J. Hu, M. Huang, C. Li, *ACS Nano* **2018**, *12*, 3424–3435.
[10] X. Fan, F. Wang, X. Ji, R. Wang, T. Gao, S. Hou, J. Chen, T. Deng, X. Li, L. Chen, et al., *Angew. Chem. Int. Ed.* **2018**, *57*, 7146–7150.
[11] J. Bitenc, R. Dominko, in *RSC Energy Environ. Ser.*, Royal Society Of Chemistry, **2019**, pp. 208–222.
[12] T. Pavčnik, J. Bitenc, K. Pirnat, R. Dominko, *Batteries & Supercaps* **2021**, *4*, 815–822.
[13] N. A. Tran, N. Do Van Thanh, M. L. P. Le, *Chem. A Eur. J.* **2021**, *27*, 9198–9217.
[14] X. Wang, H. Dong, A. Eddine Lakraychi, Y. Zhang, X. Yang, H. Zheng, X. Han, X. Shan, C. He, Y. Yao, *Mater. Today* **2022**, *55*, 29–36.
[15] A. Ponrouch, C. Frontera, F. Bardé, M. R. Palacín, *Nat. Mater.* **2016**, *15*, 169–172.
[16] S. Gheytani, Y. Liang, F. Wu, Y. Jing, H. Dong, K. K. Rao, X. Chi, F. Fang, Y. Yao, *Adv. Sci.* **2017**, *4*, 1–7.
[17] J. Bitenc, A. Scafuri, K. Pirnat, M. Lozinšek, I. Jerman, J. Grdadolnik, B. Fraisse, R. Berthelot, L. Stievano, R. Dominko, *Batteries & Supercaps* **2021**, *4*, 214–220.
[18] B. Häupler, C. Rössel, A. M. Schwenke, J. Winsberg, D. Schmidt, A. Wild, U. S. Schubert, *NPG Asia Mater.* **2016**, *8*, e283–e283.
[19] G. Fang, J. Zhou, A. Pan, S. Liang, *ACS Energy Lett.* **2018**, *3*, 2480–2501.
[20] Z. Guo, Y. Ma, X. Dong, J. Huang, Y. Wang, Y. Xia, *Angew. Chem. Int. Ed.* **2018**, *57*, 11737–11741.
[21] Q. Zhao, W. Huang, Z. Luo, L. Liu, Y. Lu, Y. Li, L. Li, J. Hu, H. Ma, J. Chen, *Sci. Adv.* **2018**, *4*, eaao1761.
[22] K. W. Nam, H. Kim, Y. Beldjoudi, T. W. Kwon, D. J. Kim, J. F. Stoddart, *J. Am. Chem. Soc.* **2020**, *142*, 2541–2548.
[23] S. Zhang, W. Zhao, H. Li, Q. Xu, *ChemSusChem* **2020**, *13*, 188–195.

[24] Z. Lin, H. Y. Shi, L. Lin, X. Yang, W. Wu, X. Sun, *Nat. Commun.* **2021**, *12*, 4424.
[25] N. Patil, C. Cruz, D. Ciurduc, A. Mavrandonakis, J. Palma, R. Marcilla, *Adv. Energy Mater.* **2021**, *11*, 2100939.
[26] N. Patil, J. Palma, R. Marcilla, *Polymers (Basel).* **2021**, *13*, 1673.
[27] Y. Gao, G. Li, F. Wang, J. Chu, P. Yu, B. Wang, H. Zhan, Z. Song, *Energy Storage Mater.* **2021**, *40*, 31–40.
[28] S. Menart, K. Pirnat, D. Pahovnik, R. Dominko, *J. Mater. Chem. A* **2023**, *11*, 10874–10882.
[29] D. J. Kim, D. Yoo, M. T. Otley, A. Prokofjevs, C. Pezzato, M. Owczarek, S. J. Lee, J. W. Choi, J. F. Stoddart, *Nat. Energy* **2019**, *4*, 51–59.
[30] D.-J. Yoo, M. Heeney, F. Glöcklhofer, J. W. Choi, *Nat. Commun.* **2021**, *12*, 2386.
[31] J. Bitenc, N. Lindahl, A. Vizintin, M. E. Abdelhamid, R. Dominko, P. Johansson, *Energy Storage Mater.* **2020**, *24*, 379–383.
[32] J. Bitenc, U. Košir, A. Vizintin, N. Lindahl, A. Krajnc, K. Pirnat, I. Jerman, R. Dominko, *Energy Mater. Adv.* **2021**, *2021*, 1–9.
[33] X. Peng, Y. Xie, A. Baktash, J. Tang, T. Lin, X. Huang, Y. Hu, Z. Jia, D. J. Searles, Y. Yamauchi, et al., *Angew. Chem. Int. Ed.* **2022**, *61*, e202203646.
[34] T. B. Schon, B. T. McAllister, P.-F. Li, D. S. Seferos, *Chem. Soc. Rev.* **2016**, *45*, 6345–6404.
[35] S. Muench, A. Wild, C. Friebe, B. Häupler, T. Janoschka, U. S. Schubert, *Chem. Rev.* **2016**, *116*, 9438–9484.
[36] M. E. Bhosale, S. Chae, J. M. Kim, J.-Y. Choi, *J. Mater. Chem. A* **2018**, *6*, 19885–19911.
[37] C. Friebe, A. Lex-Balducci, U. S. Schubert, *ChemSusChem* **2019**, *12*, 4093–4115.
[38] A. Mauger, C. Julien, A. Paolella, M. Armand, K. Zaghib, *Materials (Basel).* **2019**, *12*, 1–57.
[39] Y. Lu, J. Chen, *Nat. Chem. Rev.* **2020**, *4*, 127–142.
[40] M. Miroshnikov, K. Mahankali, N. K. Thangavel, S. Satapathy, L. M. R. Arava, P. M. Ajayan, G. John, *ChemSusChem* **2020**, *13*, 2186–2204.
[41] D. Xu, M. Liang, S. Qi, W. Sun, L. P. Lv, F. H. Du, B. Wang, S. Chen, Y. Wang, Y. Yu, *ACS Nano* **2021**, *15*, 47–80.
[42] P. Novák, K. Müller, K. S. V. Santhanam, O. Haas, *Chem. Rev.* **1997**, *97*, 207–281.
[43] Z. Song, H. Zhou, *Energy Environ. Sci.* **2013**, *6*, 2280–2301.
[44] Y. Lu, X. Hou, L. Miao, L. Li, R. Shi, L. Liu, J. Chen, *Angew. Chem. Int. Ed.* **2019**, *58*, 7020–7024.
[45] H. Chen, M. Armand, G. Demailly, F. Dolhem, P. Poizot, J.-M. Tarascon, *ChemSusChem* **2008**, *1*, 348–355.
[46] J. Xie, Z. Liang, Y.-C. Lu, *Nat. Mater.* **2020**, *19*, 1006–1011.
[47] P. Poizot, J. Gaubicher, S. Renault, L. Dubois, Y. Liang, Y. Yao, *Chem. Rev.* **2020**, *120*, 6490–6557.
[48] H. Cui, L. Ma, Z. Huang, Z. Chen, C. Zhi, *SmartMat* **2022**, *3*, 565–581.
[49] G. Dawut, Y. Lu, L. Miao, J. Chen, *Inorg. Chem. Front.* **2018**, *5*, 1391–1396.
[50] Z. Tie, L. Liu, S. Deng, D. Zhao, Z. Niu, *Angew. Chem. Int. Ed.* **2020**, *59*, 4920–4924.
[51] N. Patil, C. de la Cruz, D. Ciurduc, A. Mavrandonakis, J. Palma, R. Marcilla, *Adv. Energy Mater.* **2021**, *11*, 1–14.
[52] Z. Luo, S. Zheng, S. Zhao, X. Jiao, Z. Gong, F. Cai, Y. Duan, F. Li, Z. Yuan, *J. Mater. Chem. A* **2021**, *9*, 6131–6138.
[53] X. Geng, H. Ma, F. Lv, K. Yang, J. Ma, Y. Jiang, Q. Liu, D. Chen, Y. Jiang, N. Zhu, *Chem. Eng. J.* **2022**, *446*, 137289.
[54] H. Cui, P. Hu, Y. Zhang, W. Huang, A. Li, *ChemElectroChem* **2021**, *8*, 352–359.
[55] X. Dong, H. Yu, Y. Ma, J. L. Bao, D. G. Truhlar, Y. Wang, Y. Xia, *Chem. A Eur. J.* **2017**, *23*, 2560–2565.
[56] M. Sterby, R. Emanuelsson, X. Huang, A. Gogoll, M. Strømme, M. Sjödin, *Electrochim. Acta* **2017**, *235*, 356–364.
[57] N. Patil, A. Mavrandonakis, C. Jérôme, C. Detrembleur, N. Casado, D. Mecerreyes, J. Palma, R. Marcilla, *J. Mater. Chem. A* **2021**, *9*, 505–514.
[58] Y. Liang, Y. Jing, S. Gheytani, K.-Y. Lee, P. Liu, A. Facchetti, Y. Yao, *Nat. Mater.* **2017**, *16*, 841–848.
[59] Y. Xu, X. Wu, X. Ji, *Small Structures* **2021**, *2*, 2000113.
[60] Y. Ding, C. Zhang, L. Zhang, Y. Zhou, G. Yu, *Chem. Soc. Rev.* **2018**, *47*, 69–103.
[61] K. Hatakeyama-Sato, T. Nagano, S. Noguchi, Y. Sugai, J. Du, H. Nishide, K. Oyaizu, *ACS Appl. Polym. Mater.* **2019**, *1*, 188–196.
[62] S. Legoupy, E. Lebègue, C. Cougnon, *Electrochem. Commun.* **2016**, *70*, 47–50.
[63] A. Slesarenko, I. K. Yakuschenko, V. Ramezankhani, V. Sivasankaran, O. Romanyuk, A. V. Mumyatov, I. Zhidkov, S. Tsarev, E. Z. Kurmaev, A. F. Shestakov, et al., *J. Power Sources* **2019**, *435*, 226724.
[64] V. V. Pavlishchuk, A. W. Addison, *Inorg. Chim. Acta* **2000**, *298*, 97–102.
[65] S. Aldrich, "Ag/AgCl (3 M NaCl) Reference Electrode," can be found under https://www.sigmaaldrich.com/SI/en/product/aldrich/basmf2052, **2023**.
[66] K. Hernández-Burgos, G. G. Rodríguez-Calero, W. Zhou, S. E. Burkhardt, H. D. Abruña, *J. Am. Chem. Soc.* **2013**, *135*, 14532–14535.
[67] N. Patil, A. Mavrandonakis, C. Jérôme, C. Detrembleur, J. Palma, R. Marcilla, *ACS Appl. Energ. Mater.* **2019**, *2*, 3035–3041.
[68] H. Hotta, M. Ueda, S. Nagano, Y. Tsujino, J. Koyama, T. Osakai, *Anal. Biochem.* **2002**, *303*, 66–72.
[69] A. Kiani, J.-B. Raoof, D. Nematollahi, R. Ojani, *Electroanalysis* **2005**, *17*, 1755–1760.
[70] Y. Xu, Y.-H. Wen, J. Cheng, G.-P. Cao, Y.-S. Yang, *Electrochim. Acta* **2010**, *55*, 715–720.
[71] J. D. Benck, B. A. Pinaud, Y. Gorlin, T. F. Jaramillo, *PLoS One* **2014**, *9*, e107942.
[72] D. Jürgen, E. Steckhan, *J. Electroanal. Chem.* **1992**, *333*, 177–193.
[73] A. L. Beilby, T. A. Sasaki, H. M. Stern, *Anal. Chem.* **1995**, *67*, 976–980.
[74] A. Dekanski, J. Stevanović, R. Stevanović, B. Ž Nikolić, V. M. Jovanović, *Carbon* **2001**, *39*, 1195–1205.
[75] G. K. Kiema, M. Aktay, M. T. McDermott, *J. Electroanal. Chem.* **2003**, *540*, 7–15.
[76] Q.-L. Zhao, Z.-L. Zhang, L. Bao, D.-W. Pang, *Electrochem. Commun.* **2008**, *10*, 181–185.
[77] H. A. Anderson, R. H. Thomson, *J. Chem. Soc. C* **1967**, 2152–2155.
[78] J. Y. Savoie, P. Brassard, *Can. J. Chem.* **1969**, *47*, 733–737.
[79] Y. A. Sayapin, Z. N. Bang, V. N. Komissarov, I. V. Dorogan, V. V. Tkachev, G. V. Shilov, S. M. Aldoshin, V. I. Minkin, *Russ. J. Org. Chem.* **2009**, *45*, 1663–1669.
[80] K. Pirnat, N. Casado, L. Porcarelli, N. Ballard, D. Mecerreyes, *Macromolecules* **2019**, *52*, 8155–8166.
[81] Y. Liang, P. Zhang, S. Yang, Z. Tao, J. Chen, *Adv. Energy Mater.* **2013**, *3*, 600–605.
[82] Y. Liang, P. Zhang, J. Chen, *Chem. Sci.* **2013**, *4*, 1330–1337.
[83] J. E. Bachman, L. A. Curtiss, R. S. Assary, *J. Phys. Chem. A* **2014**, *118*, 8852–8860.
[84] K. Hernández-Burgos, S. E. Burkhardt, G. G. Rodríguez-Calero, R. G. Hennig, H. D. Abruña, *J. Phys. Chem. C* **2014**, *118*, 6046–6051.

Manuscript received: September 25, 2024
Revised manuscript received: December 13, 2024
Version of record online: January 5, 2025